Noise suppression for the detection laser of a nuclear magnetic resonance gyroscope based on a liquid crystal variable retarder

Binquan Zhou (周斌权)[1,2], Guanqun Lei (雷冠群)[1,2], Linlin Chen (陈琳琳)[1,2], Wenfeng Wu (吴文峰)[1,2], Zhuo Wang (王 卓)[1,2,*], Xiaofeng Meng (孟晓风)[1,2], and Jiancheng Fang (房建成)[1,2]

[1]*School of Instrumentation Science and Opto-Electronics Engineering, Beihang University, Beijing 100191, China*
[2]*Key Laboratory on Inertial Technology, Beijing 100191, China*
**Corresponding author: zhuowang@buaa.edu.cn*

Received January 6, 2017; accepted May 19, 2017; posted online June 12, 2017

In this Letter, the liquid crystal variable phase retarder is applied for the accurate modulation of the laser power in a detection system and the construction of a system that suppresses the influence of laser noise on the gyro's bias instability. A closed-loop control method for a laser noise suppression system is proposed. We obtain a power stability index of 0.038% in a 3-h continuous test, and the nuclear magnetic resonance gyroscope bias instability reaches 1°/h. The proposed control method effectively improves the signal-to-noise ratio of the gyroscope detection signal, which lays the technical foundation for future research work.

OCIS codes: 230.0230, 020.0020.
doi: 10.3788/COL201715.082302.

Nuclear magnetic resonance gyroscopes (NMRGs) are a kind of rotation-speed sensor that senses the angular velocity by measuring a frequency shift in the Larmor precession of the nuclear spin in a constant magnetic field[1–6]. Its bias instability is expected to be 0.01°/h[7]. The NMRG is insensitive to vibrations. They have the potential advantages of lower cost of manufacture, a smaller size, and higher precision. The spin polarization of the noble gas atoms influences the signal-to-noise ratio (SNR) of the NMRG, which is proportional to the laser stability[8–13]. The improvement of the laser intensity stability can promote the SNR of the signal detected by the magnetic resonance gyroscope. There are two main methods of stabilizing the power of semiconductor lasers[14–16]. One method is to achieve a controllable laser output by controlling the temperature and current injection of the laser. However, this method has no control ability on the power fluctuation caused by other factors, and the power stability is around 1%. The other method is to modulate the laser beam directly by using the external optical modulator, such as an acoustic optical modulator, an electro-optical modulator, etc.[17–19], and to suppress the power fluctuation of the laser by using negative feedback. The power stability of such a method is in the magnitude of 10^{-4}. Other studies on laser power fluctuations are also numerous[20,21].

A liquid crystal variable retarder (LCVR) can be used to modulate the laser intensity[22,23]. Compared with other optical modulating devices, the LCVR has the advantages of a small volume, low working voltage, and large clear aperture, etc. A device comprised of an LCVR and a polarization plate can achieve laser power stability through negative feedback[24–29]. For this purpose, a special LCVR driving system has been designed so as to achieve stable control of the LCVR, with an acquired 3-h power stability of about 0.038%, and with the NMRG bias instability reaching 1°/h. This has improved the SNR of NMRGs effectively and has laid the technical foundation for the subsequent research work[30–34].

The NMRG is a kind of atomic gyroscope designed on the principle of nuclear magnetic resonance. The principle for the angular rate ω_R to be detected by the magnetic resonance gyroscope shall be[1,3,4]

$$\omega_R = \omega'_L - \omega_L, \tag{1}$$

where ω'_L is the Larmor procession frequency of the nucleon obtained from the detection signal of the photoelectric detector. ω_L is the Larmor procession frequency of the nucleon, which is determined by an applied magnetic field intensity B_0 and the gyromagnetic ratio γ of the nucleus itself, and[3]

$$\omega_L = \gamma B_0. \tag{2}$$

The pumping laser and detecting laser shall be used in the operation of the magnetic resonance gyroscope. Firstly, the electron inside the alkali metal shall be driven into a polarized state with a pumping laser. Then, the status information of the atom shall be obtained through the detecting laser, and the angular rate information of the carrier can be obtained through signal processing.

To measure the angular rate of the carrier with an NMRG, it is first necessary to obtain the information of the detecting laser passing the alkali-metal air chamber through the photoelectric detector. From the information of the detecting laser, the x component $\delta M_x^{(Rb)}$ of the

electronic magnetic moment can be obtained, and the x component M_x of the nucleon magnetic momentum can be obtained through the signal demodulation processing for it:

$$M_x = M_0 \gamma B_1 T_2 \sin(\omega_a t + \Delta\varnothing), \tag{3}$$

where M_0 is the electronic magnetic moment in the z-axis direction, which is the amplitude of the x-direction alternating magnetic field. T_2 is the transverse relaxation time of the nucleon, and ω_a is the field frequency on the x-axis.

The demodulated signal is, therefore,

$$M_{x(\text{demod})} = \frac{M_0 \gamma B_1 T_2}{2}\left(1 - \frac{\Delta\varnothing^2}{2}\right). \tag{4}$$

Then, the angular rate ω_R of the carrier can be measured through the equation $\Delta\varnothing = \Delta\omega_R t$, as shown in Fig. 1. The detecting laser of the NMRG is the linearly polarized light from the x-axis incidence, and the x component $M_x^{(Rb)}$ of the electronic magnetic moment shall be in direct proportion to the alternating component of the light intensity of the detecting laser:

$$\delta I_x \propto M_x^{(Rb)}. \tag{5}$$

Therefore, the noise of the detecting laser is certain to result in the instability of the x component $M_x^{(Rb)}$ of the electronic magnetic moment, which will further introduce measuring noise in obtaining the angular rate ω_R of the carrier.

The LCVR is a wave plate with continuously adjustable phase retardation produced by the electro-optic birefringent effect of the nematic liquid crystal. The molecule of the nematic liquid crystal has a birefringent effect, and its refractive index difference is mainly related to the voltage (denoted as V) applied to it. The structure of the LCVR mainly includes a fusion quartz substrate, an indium-tin-oxide film, an insulation array layer, and a nematic liquid crystal.

The phase retardation of the LCVR can be expressed as $\delta = 2\pi\Delta n t/\lambda$, where Δn is the refractive index difference of the crystal, which is relevant to the voltage, crystal material, and temperature. The unit of δ is rad. $\Delta l = \Delta n t$ is denoted as the optical path difference produced in the crystal; then, $\delta = 2\pi\Delta l/\lambda$. Therefore, for transmission light with a certain wavelength, the optical path difference is in one-to-one correspondence with the phase retardation.

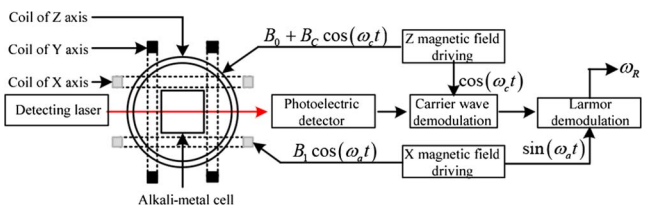

Fig. 1. Diagram of second demodulation process of ω_R.

The change relation between δ and V is shown in Fig. 2(a). When it has no voltage function, δ is the maximum, which is denoted as δ_0. When V is smaller, δ almost does not change δ_0. If V exceeds the threshold value V_c, δ shall be decreased, obviously, with the increase of V. When V is large enough, then δ shall be very small. The residual optical path difference of ~30 nm still exists. This study adopts the Thorlabs LCC1111-B-type half-wave LCVR, which is applicable to the near-infrared band. $\delta_0 > \pi$ exists in any transmission light within such a wave band.

The schematic diagram of a liquid-crystal variable laser power attenuator based on the LCVR is shown in Fig. 3. The polarizer is in quadrature with the transmitting axis

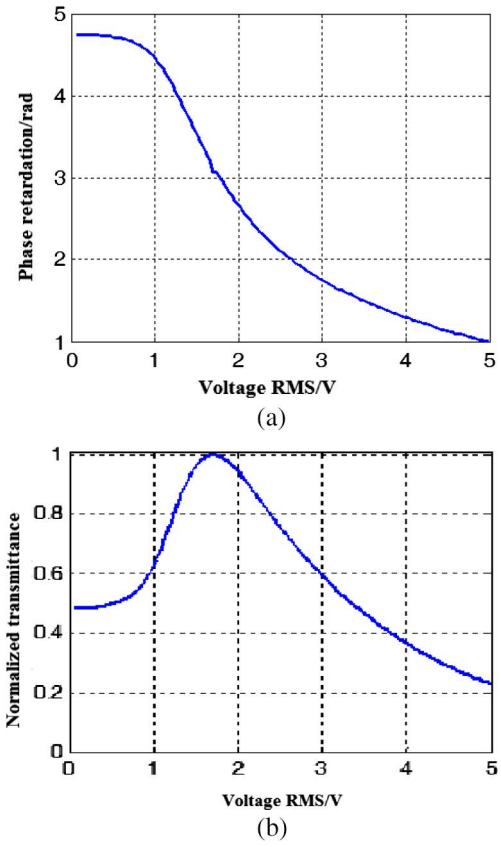

Fig. 2. LCVR phase retardation and transmittance. (a) Change relationship between LCVR phase retardation and voltage and (b) change relationship between unified transmittance and voltage.

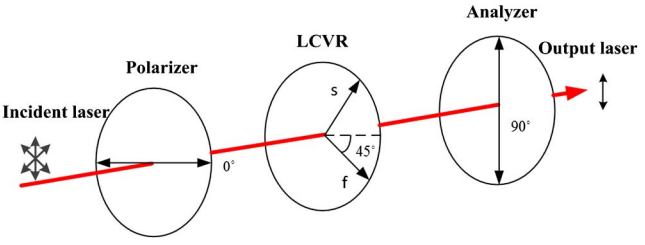

Fig. 3. Schematic diagram of the liquid crystal variable attenuator.

of the analyzer, and the fast axis of the LCVR is 45° with the transmitting axis of the polarizer. When $V = V_{\lambda/2}$, the LCVR shall have a $\lambda/2$ optical path difference; thus $V_{\lambda/2}$ is called the half-wave voltage of the LCVR. The polarization direction of linearly polarized light emitted from the polarizer is rotated 90° by the LCVR, and the laser power emitted from the analyzer shall reach the maximum level. If V keeps increasing, then δ shall decrease continually. When V is large enough, δ shall be close to 0, and the laser polarization direction emitted from the polarizer shall be in quadrature with the transmitting axis of the analyzer, and the output light power is the weakest.

The polarization direction of incident light shall be adjusted into the horizontal polarization light; when the polarizer will not work, it can be omitted. The incident light power shall be denoted as I_0; then, the emergent light power shall be $I = I_0 \sin^2(\delta/2)$[25]. The normalized transmittance of the liquid-crystal variable power attenuator can be denoted as $I_{\text{norm}} = I/I_0 = \sin^2(\delta/2)$. The change relation between it and the voltage is shown in Fig. 2(b). If $V \geq V_{\lambda/2}$, then $\delta \in (0 \times \pi]$, $I_{\text{norm}} \in (0 \times 1]$, and I_{norm} shall be in monotone, decreasing with the increase of V.

The laser power stabilization system based on the LCVR uses the above liquid-crystal variable power attenuator as the actuator, which stabilizes the laser power through negative feedback control by using the photodiode-sampling laser power signal. When I_0 increases, then the driving system will make V increase, and I_{norm} will decrease so as to maintain $I_0 = I_0 \cdot I_{\text{norm}}$. On the contrary, when I_0 decreases, the driving system will make V decrease. When V decreases to $V_{\lambda/2}$, the normalized transmittance reaches the maximum; if I still cannot reach the setup value at this moment, then the system shall run out, and stable power cannot be achieved. Therefore, the power setup value of the system must be smaller than the minimum within the original laser-power fluctuation range. The system shall sacrifice partial laser power to obtain the improvement in output laser power stability.

Figure 4 shows the schematic diagram for the testing device for the stability test of the LVCR laser power.

The optical axis of the polarizer is perpendicular to the optical axis of the polarizer. The angle between the optical axis of the polarizer and the fast axis of the liquid crystal variable phase retarder is 45°. The laser generates a linear polarized light with a wavelength of 795 nm and a power of about 1 mW, which is separated by a beam splitter (BS1) and received by a photo detector (PD3). The PD3 receiving laser is mainly used to monitor the original intensity information. Another beam of light enters a variable laser power attenuator formed by a polarizer, a liquid crystal variable phase retarder, and a polarizer. By changing the driving voltage applied to the LCVR, the polarization state of the laser can be changed so as to change the output power of the laser. The laser emitted from the detector is divided into two beams by BS2. The detector PD1 is used for the sampling of the optical power, and the detector PD2 is used to test the stability of the output laser power. The optical power sampled from PD1 is converted to a voltage signal in the control unit. The control unit compares the actual optical power with a set value to produce the appropriate control voltage. At the same time, a symmetrical square wave signal with a frequency of 2 kHz, a duty cycle of 50%, and an average value of 0 is generated in the circuit. The amplitude of the square wave is modulated by the control voltage, which is loaded on the liquid-crystal controllable phase retarder, and the optical power of the outgoing laser is changed to realize the closed-loop stability of the power.

The results of continuous 3-h testing on the system are shown in Fig. 5. The original light intensity and the laser intensity after stabilization shall be normalized to their mean values separately after stabilization. The light intensity stabilization shall be balanced with standard deviation; then, the original light intensity stabilization is about 7.6%. After the stabilization, the stabilization of the laser light intensity shall be about 0.038%. The nominal stability of the laser noise attenuator of goods from Thorlabs is 0.05%. It can be seen that the driving system designed in the Letter can achieve the stabilization of the light power better.

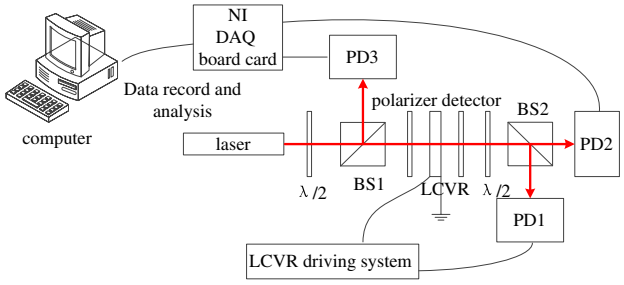

Fig. 4. Schematic diagram of the laser intensity stabilization system.

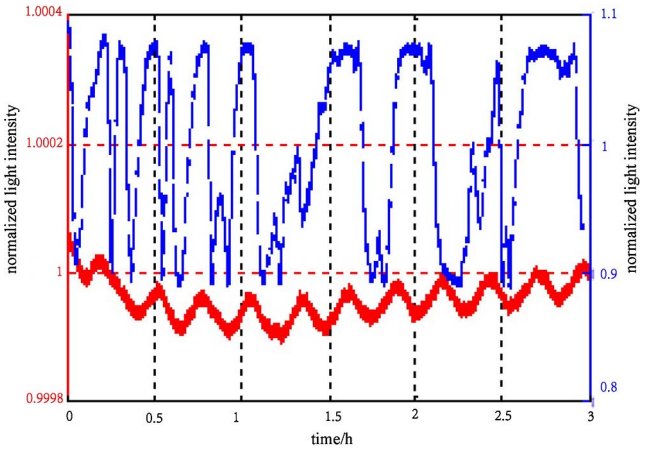

Fig. 5. (Color online) Results of laser inspection system stabilization experiment.

In order to compare the effect of the laser power on the detection of the NMRG, a stability test of the NMRG detection signal was carried out on the NMRG prototype. It is known that the angular rate ω_R of the carrier is achieved by measuring the x component M_x of the nucleon magnetic momentum. Therefore, a contrast experiment is designed to test whether the laser power is stable to the NMRG detection signal.

The results of the x component M_x of the nucleon magnetic momentum where the detecting laser has not achieved power stability are shown in Fig. 6, and the standard deviation is 0.031%. The results of the x weight M_x of the nucleon magnetic momentum where the detecting laser has achieved power stability are shown in Fig. 7, and the standard deviation is 0.014%. It can be seen that after the detecting laser achieves power stability, the amplitude stability of x weight M_x of the nucleon magnetic momentum of the magnetic resonance gyroscope can be improved.

Figure 8 shows the spectrum analysis diagram of the detection signal of the NMRG where the detecting laser has or has not achieved power stability. It can be seen that after the detecting laser achieves power stability, the noise baseline of the detection signal decreases obviously, which greatly increases the SNR of the detection signal of the NMRG.

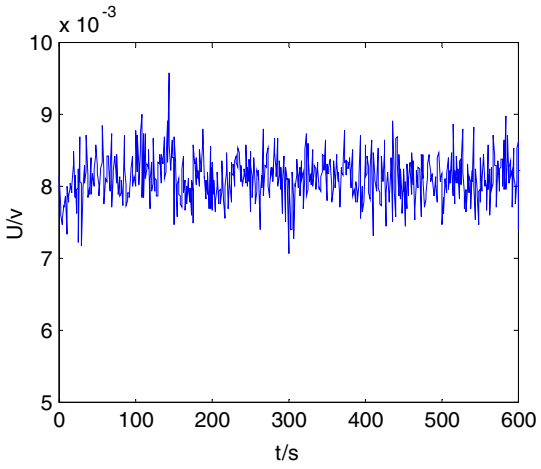

Fig. 6. Results of the laser without intensity stabilization.

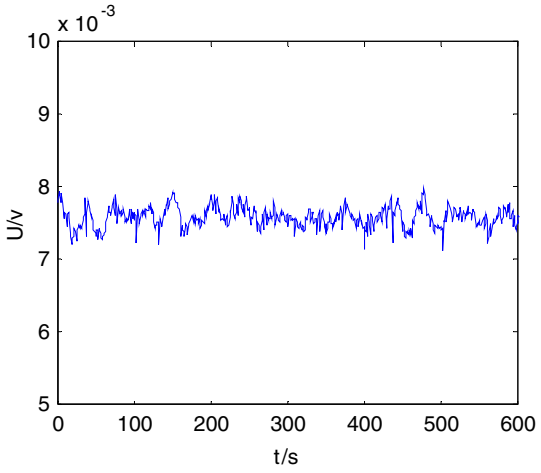

Fig. 7. Results of the laser with intensity stabilization.

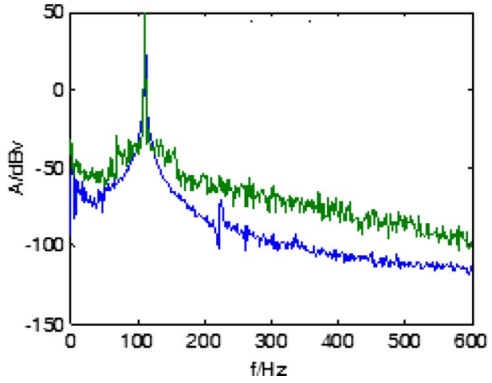

Fig. 8. (Color online) Detection signal spectrum analysis.

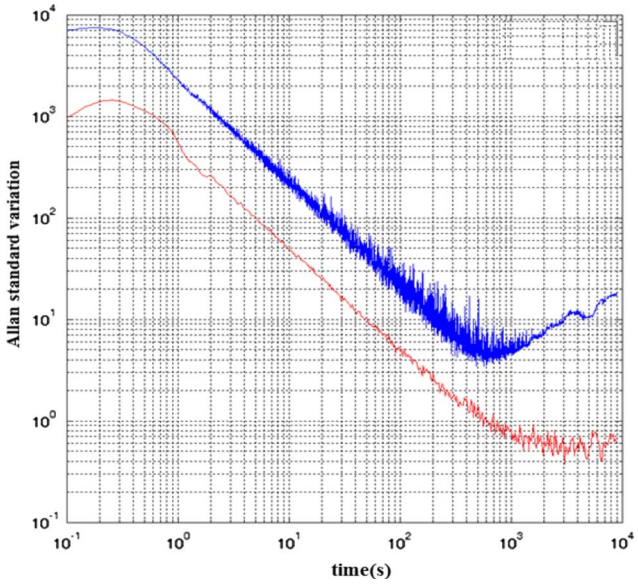

Fig. 9. (Color online) Allan standard deviation curve.

It can be seen from Fig. 9 that the short-term stability has been obviously promoted after the NMRG restrains the detecting noise, which is mainly due to the promotion of the SNR of the detection signal, and the gyroscope bias instability can reach 1°/h, laying a good technical foundation for the promotion of detection precision and the gyroscope index.

The Letter analyzes the relationship between the power stability of a detecting laser of an NMRG and the noise of the detecting laser signal, which introduces the working principle of the laser-power stability system based on the LCVR, and proposes the closed-loop control method for the laser noise suppression system by design of the circuit control system. By using such a system, the precision test for the NMRG is carried out, and a power stability index of 0.038% is achieved in 3-h continuous testing.

The SNR of the detection signal of the NMRG is improved effectively, and the bias instability achieves an index of 1°/h, laying the technical foundation for subsequent research.

This work was supported by the National Natural Science Foundation of China (Nos. 61673041, 61673041, and 61227902) and the National High Technology Research and Development Program 863 (No. 2014AA123401).

Author Contributions: Yueyang Zhai and Zhaohui Hu conceived and designed the experiments, Wei Quan performed the experiments, and Qing Liang analyzed the data.

References

1. D. Tazartes, in *IEEE International Symposium on Inertial Sensors and Systems* (2014).
2. T. W. Kornack, R. K. Ghosh, and M. V. Romalis, Phys. Rev. Lett. **95**, 23 (2005).
3. M. Larsen and M. Bulatowicz, in *IEEE International Frequency Control Symposium Proceedings* (2012).
4. J. Kitching, S. Knappe, and E. A. Donley, IEEE Sens. J. **11**, 9 (2011).
5. X. H. Liu, H. Luo, T. L. Qu, K. Y. Yang, and Z. C. Ding, AIP Adv. **5**, 10 (2015).
6. J. C. Fang and J. Qin, Sensors **12**, 5 (2012).
7. D. Meyer and M. Larsen, Gyroscopy Navig. **5**, 2 (2014).
8. W. Loh, M. T. Hummon, H. F. Leopardi, T. M. Fortier, F. Quinlan, J. Kitching, S. B. Papp, and S. A. Diddams, Opt. Express **24**, 13 (2016).
9. E. Oh, R. A. Horne, and C. A. Sackett, Rev. Sci. Instrum. **87**, 6 (2016).
10. A. Al-Masoudi, S. Dorscher, S. Hafner, U. Sterr, and C. Lisdat, Phys. Rev. A **92**, 6 (2015).
11. K. Saleh, J. Millo, A. Didier, Y. Kersale, and C. Lacroute, Appl. Opt. **54**, 32 (2015).
12. B. T. R. Christensen, M. R. Henriksen, S. A. Schaffer, P. G. Westergaard, D. Tieri, J. Ye, M. J. Holland, and J. W. Thomsen, Phy. Rev. A **92**, 5 (2015).
13. B. Cheng, Z. Y. Wang, B. Wu, A. P. Xu, Q. Y. Wang, Y. F. Xu, and Q. Lin, Chin. Phys. B **23**, 10 (2014).
14. A. Lezama, R. Rebhi, A. Kastberg, S. Tanzilli, and R. Kaiser, Phys. Rev. A **92**, 3 (2015).
15. B. Z. Tan, Y. Tian, H. F. Lin, J. H. Chen, and S. H. Gu, Opt. Lett. **40**, 16 (2015).
16. R. J. Li, W. F. Fan, L. W. Jiang, L. H. Duan, W. Quan, and J. C. Fang, Phys. Rev. A **94**, 3 (2016).
17. K. W. Li, Z. B. Wang, Y. H. Chen, C. Q. Yang, and R. Zhang, Acta Phys. Sin. **64**, 18 (2015).
18. L. Zhao and Q. Zhao, Chin. Opt. Lett. **8**, 107 (2010).
19. O. Kalman, Z. Darazs, F. Brennecke, and P. Domokos, Phys. Rev. A **93**, 3 (2016).
20. X. Fang, S. Yuan, W. Liu, B. Yan, and B. Huang, Chin. Opt. Lett. **13**, 033101 (2015).
21. W. Qi, Y. Jiang, X. Li, L. Jin, Z. Bi, and L. Ma, Chin. Opt. Lett. **14**, 101401 (2016).
22. P. Oxley and J. Wihbey, Rev. Sci. Instrum. **87**, 9 (2016).
23. Y. Zhang, H. J. Zhao, and X. Cheng, Spectrosc. Spectral Anal. **31**, 5 (2011).
24. Y. L. Wang, R. Zhang, and Z. B. Wang, Spectrosc. Spectral Anal. **35**, 8 (2015).
25. J. M. López-Téllez and N. C. Bruce, Proc. SPIE **8785**, 87852J (2013).
26. L. J. Salazar-Serrano, D. Janner, N. Brunner, V. Prunei, and J. Torres, Phys. Rev. A **89**, 1 (2014).
27. K. D. Quoc, Opt. Quantum Electron. **48**, 6 (2016).
28. J. Kong, V. G. Lucivero, R. Jimenez-Martinez, and M. W. Mitchell, Rev. Sci. Instrum. **86**, 7 (2015).
29. T. V. Radina, Phys. Rev. A **379**, 36 (2015).
30. S. Knappe, V. Shah, P. Schwindt, and J. Kitching, Appl. Phys. Lett. **85**, 9 (2004).
31. I. A. Sulai, R. Wyllie, M. Kauer, G. S. Smetana, R. T. Wakai, and T. G. Walker, Opt. Lett. **38**, 6 (2013).
32. L. L. Yan, J. Q. Zhang, J. Jing, and M. Feng, Phys. Rev. A **379**, 39 (2015).
33. P. Bushev, G. Hetet, L. Slodicka, D. Rotter, M. A. Wilson, F. Schmidt-Kaler, J. Eschner, and R. Blatt, Phys. Rev. Lett. **110**, 13 (2013).
34. C. X. Zhu, Y. Y. Feng, X. Y. Ye, Z. Y. Zhou, Y. J. Zhou, and H. B. Xue, Acta Phys. Sin. **57**, 2 (2008).